



## OPEN The PI3K-AKT-mTOR signaling pathway mediates epithelial mesenchymal transition and cytoskeletal architecture changes induce to renal fibrosis after Bisphenol S exposure

Zhaoxia Zhang<sup>1</sup>, Liming Jin<sup>2,3,4</sup>, Tao Mi<sup>2,3,4</sup>, Jinkui Wang<sup>2,3,4</sup>, Zhaoying Wang<sup>2,3,4</sup>, Junyi Luo<sup>2,3,4</sup>, Chunnian Ren<sup>2,3,4</sup>, Xin Wu<sup>2,3,4</sup>, Jiayan Liu<sup>2,3,4</sup>, Peng Guo<sup>2,3,4,5</sup>, Li Wang<sup>1</sup>✉ & Dawei He<sup>1</sup>✉

Bisphenol S (BPS) is considered a good substitute for bisphenol A (BPA) in industrial applications, and data suggest that the kidney is an important injury site after BPS exposure. However, the phenotype of kidney injury induced by BPS exposure and the mechanism of its damage remain unknown. Therefore, this study aims to investigate the phenotype and specific mechanism of kidney injury induced by BPS exposure. SD rats are treated with three different doses of BPS (50 mg/kg body weight (b.w.), 100 mg/kg b.w., and 150 mg/kg b.w.), and HK-2 cells are treated with 100  $\mu$ M BPS, 200  $\mu$ M and 400  $\mu$ M BPS to mimic the in vitro and in vivo environment of BPS exposure-induced kidney injury. Meanwhile, the potential mechanism of BPS exposure-induced kidney injury was screened by RNA sequencing and further verified by in vitro experiments. BPS exposure induces cytoskeletal architecture damage and EMT transformation in HK-2 cells, promoting renal fibrosis. In addition, it was found that activation of the PI3K-AKT-mTOR signaling pathway plays a key role in cytoskeletal architecture damage and EMT transformation in HK-2, and after inhibition of PI3K-AKT-mTOR signaling by Wortmannin, the cytoskeletal architecture disorders, and EMT are partially reversed. In conclusion, we found that the activation of the PI3K-AKT-mTOR signaling pathway can mediate disturbed cytoskeletal architecture and EMT to induce renal fibrosis after BPS exposure.

**Keywords** Bisphenol S, Cytoskeleton, EMT, Fibrosis

At present, environmental pollution has seriously threatened human health. Damage from environmental pollutants, including PM2.5/microplastics/DEHP/BPA, is a current research hotspot. As a common ingredient in polycarbonate plastics and epoxy resin, bisphenol A (BPA) is one of the most productive chemical production products in the world<sup>1</sup>. It is widely used in a variety of packaging materials toys and containers and other consumer goods<sup>2,3</sup>. BPA exposure has been demonstrated to cause damage to multiple systems including reproduction, endocrine, and circulation<sup>4–6</sup>. Because of the huge health risks associated with BPA, many regulators have banned its use. Bisphenol S (BPS; 2,2–2 [4-hydroxyphenol] sulfone) is considered a good alternative to BPA

<sup>1</sup>Department of Paediatrics, The Second Affiliated Hospital of Chongqing Medical University, Chongqing 400014, People's Republic of China. <sup>2</sup>Department of Urology, Children's Hospital of Chongqing Medical University, Chongqing 400014, People's Republic of China. <sup>3</sup>Chongqing Key Laboratory of Children Urogenital Development and Tissue Engineering, Chongqing 400014, People's Republic of China. <sup>4</sup>China International Science and Technology Cooperation Base of Child Development and Critical; National Clinical Research Center for Child Health and Disorders, Chongqing; Ministry of Education Key Laboratory of Child Development and Disorders, Chongqing Key Laboratory of Pediatrics, Chongqing 400014, People's Republic of China. <sup>5</sup>Institute of Basic Medicine and Cancer (IBMC), Chinese Academy of Sciences, Hangzhou 310022, Zhejiang, People's Republic of China. ✉email: liwang8771@126.com; hedawei@hospital.cqmu.edu.cn

in industrial applications and has gradually replaced BPA in canned and other prepackaged foods<sup>7</sup>. The ECHA conducted a market survey and found that BPS production had doubled (from 200 tons to 397 tons) between 2016 and 2017 alone<sup>8</sup>. The researchers found that BPS had almost 100 times higher solubility in water than BPA, making it easy to detect BPS in aqueous environments<sup>9</sup>. Moreover, BPS is more difficult to degrade than BPA and significantly accumulates in humans and biota<sup>10</sup>. The daily dietary intake of BPS in US adults is reported to be 1.31 ng/kg<sup>7</sup>. Because of the similar structure of BPS to BPA and its unrestricted production or application, it is now considered an environmental pollutant<sup>11</sup>, and its safety is also widely controversial.

Chronic kidney disease (CKD) affects approximately 10% of both the European and US populations<sup>2,12</sup>. Organ fibrosis significantly contributes to global mortality, with estimates suggesting it causes a 50% increase in deaths in developing countries<sup>13</sup>. Renal fibrosis is linked to a decline in kidney function and represents the final common pathway for all types of chronic kidney injury<sup>14</sup>. Various factors can lead to renal fibrosis, including certain drugs. For instance, aristolochic acid can result in progressive renal interstitial fibrosis<sup>15</sup>, while calcium oxalate can trigger epithelial-to-mesenchymal transition (EMT) in tubular epithelial cells<sup>16</sup>. Additionally, obstructive factors, such as unilateral ureteral obstruction (UUO), can mimic chronic obstructive kidney disease and also lead to renal fibrosis<sup>17,18</sup>.

The EMT is a dynamic process in which epithelial cells transform into mesenchymal cells. EMT and its intermediate states are considered key contributors to organ fibrosis. The cytoskeletal architecture, made up of microtubules, microfilaments, and intermediate filaments, is a dynamic and adaptive network that governs cell movement and morphology, while also facilitating communication between the cell and its extracellular environment. The polymers that form the cytoskeleton, along with their regulatory proteins, constantly undergo reorganization in response to various stimuli that promote biological processes and functions. During sustained EMT, there is a reorganization of epithelial cytokines, resulting in loss of cell polarization, disruption of cell-to-cell junctions, degradation of the basement membrane, and reorganization of the extracellular matrix (ECM). These changes make the cells more aggressive<sup>19</sup>. The EMT process is regulated by several signaling pathways, with the PI3K-AKT-mTOR pathway playing a particularly important role. Activation of the mTOR complex 1 (mTORC1) and complex 2 (mTORC2) regulates cytoskeletal rearrangement. Conversely, inhibiting PI3K can prevent the kidneys from undergoing EMT, highlighting the critical role of the PI3K-AKT pathway in this process<sup>20,21</sup>. During EMT, mTORC1 is involved in increasing cell size, protein synthesis, motility, and invasion, while mTORC2 is essential for the transition from epithelial to mesenchymal cells.

Previous studies have demonstrated the toxic effects of BPA on the kidneys. Long-term administration of BPA in healthy mice can lead to renal injury, characterized by inflammatory infiltrates and tubular fibrosis<sup>22</sup>. Additionally, BPA promotes mitochondrial damage and cell death in renal tubular cells, which exacerbates renal injury<sup>23</sup>. As a substitute for BPA, the safety of BPS exposure on renal health also warrants attention. Previous research indicates that BPS can cause renal histopathological disturbances in Wistar rats, altering serum and urine biomarkers related to renal injury<sup>24</sup>. Furthermore, BPS found in dialysis materials increases the burden on kidney patients<sup>25</sup>, highlighting that renal injury due to BPS is a clinical concern. Despite this, few studies have focused on the specific phenotype and mechanisms of renal injury caused by BPS exposure. Therefore, in this study, we aimed to simulate BPS exposure-induced renal injury through *in vitro* and *in vivo* experiments. We also conducted RNA sequencing to identify potential damage mechanisms, providing a theoretical basis for understanding BPS exposure-induced renal injury and raising social awareness about the safety of BPS.

## Methods and materials

### Chemicals

The BPS used in the animal experiments (CAS No. 1478-61-1, > 98% purity) was prepared using the same method as outlined in previous literature<sup>26</sup>. For the cell experiments, BPS (CAS No. 80-09-1) was obtained from Sigma Chemical Reagents, USA. It was diluted using dimethyl sulfoxide (DMSO) and the culture medium, ensuring that the final concentration of DMSO remained below 0.1%.

### Animal models and interventions

A total of 24 adult male Sprague-Dawley (SD) rats were obtained from the Experimental Animal Center at Chongqing Medical University in Chongqing, China. The animals were maintained under specific pathogen-free (SPF) conditions, with access to adequate food and distilled water. Previous studies suggest that the saturation of the metabolic and clearance pathways of BPS in rats may begin at a dosage of 110 mg/kg b.w. or lower<sup>27</sup>. Therefore, our study included four groups: a control group (receiving equal amounts of ethanol and corn oil), and treatment groups receiving 50 mg/kg b.w., 100 mg/kg b.w., and 150 mg/kg b.w. of BPS. The rats were administered the treatment daily for 35 consecutive days. On day 36, the rats were euthanized by CO<sub>2</sub> inhalation, and their kidneys were subsequently removed. Venous blood was also collected for biochemical analysis. The left kidney was placed in liquid nitrogen for future experiments, while the right kidney was preserved in 4% paraformaldehyde for immunohistochemistry and immunofluorescence studies. The Laboratory Animal Welfare Ethics Review Committee of the Children's Hospital of Chongqing Medical University approved this animal experiment (license no. CHCMU-AICUC20220323004).

### Biochemical assays and Masson trichrome staining

Immediately following the rat sacrifice, whole blood was collected to assess blood urea nitrogen (BUN) and serum creatinine (SCr) levels. The method used was similar to that in our previous work<sup>28</sup>. Kidney tissue was routinely fixed and dehydrated to prepare paraffin sections. These sections were then stained using a Masson's trichrome staining kit and examined under a microscope.

### Immunohistochemistry

Kidney tissue sections were routinely dewaxed and underwent antigen retrieval. They were then blocked with 0.5% BSA for 1 h before being incubated with the primary antibody overnight. Afterward, the sections were washed three times with PBS, followed by incubation with the corresponding secondary antibody. The samples were then stained with DAB and hematoxylin, and finally dehydrated. Specific steps are detailed in the previous study<sup>22</sup>. Antibody information can be found in Supplementary Table 1.

### Cell culture

The HK-2 cell (Cat. No. TCH-C400) was obtained from the Shanghai Cell Bank. Cell cultures were conducted using DMEM/F12 medium supplemented with 10% FBS and penicillin-streptomycin, under culture conditions of 37 °C with 5% CO<sub>2</sub>.

### The assay of cell viability

Cell viability was assessed using the CCK-8 assay to determine the appropriate concentrations for subsequent experiments. HK-2 cells were seeded in 96-well plates and exposed to different concentrations of BPS: 0, 10, 50, 100, 200, 400, 800, 1600, and 3200 μM. After 24 h, a CCK-8 working solution was added, and the incubation continued for an additional 2 h. Finally, the optical density (OD) at 450 nm was measured using a spectrophotometer.

### Cell morphology and scratch assay

The cell experiment included four groups: a control group, and groups treated with 100 μM, 200 μM, and 400 μM BPS. After 24 h, photographs were taken under a microscope to observe the morphology of HK-2 cells. The method for the scratch experiments was similar to our previous work<sup>29</sup>.

### Immunofluorescence

HK-2 cells were added to 24-well plates containing pre-prepared cell-climbing slices and subsequently treated with BPS. Immunofluorescence detection was performed after 24 h. Kidney tissues were routinely fixed, dehydrated, and embedded in paraffin sections in preparation for immunofluorescence detection. The immunofluorescence method is described in our previous work<sup>28</sup>. Antibody information can be found in Supplementary Table 1.

### Western blotting

The protein extraction method and the Western blot protocol were consistent with our previous study<sup>16</sup>. Image acquisition and densitometry analyses were conducted using Image Lab (version 6.0.0, USA). All antibody details can be found in Supplementary Table 1.

### Cytoskeleton detection

The cytoskeletal architecture was examined using two markers: filamentous actin(F-actin) and β-tubulin. F-actin was stained with Rhodamine-labeled phalloidin, following specific procedures as previously described<sup>26</sup>. Image acquisition was conducted using the A1R confocal microscopy system (Nikon, Tokyo, Japan). β-Tubulin staining was performed using the same protocol as cellular immunofluorescence staining.

### Wortmannin (PI3K inhibitor) and Sapanisertib (mTORC inhibitor) treatment

The PI3K inhibitor Wortmannin (CAS No. 19545-26-7, MCE) and the mTORC inhibitor Sapanisertib (CAS No. 1224844-38-5) were dissolved in dimethyl sulfoxide (DMSO), ensuring the final concentration of DMSO was less than 0.1%. In the cell rescue assay, we used 10 μM Wortmannin and 1 nM Sapanisertib.

### RNA sequencing (RNA-seq)

A total of six kidney samples were randomly chosen from both the control group and the group treated with 100 mg/kg b.w. of BPS. Additionally, HK-2 cells were selected from the control group and the group treated with 200 μM of BPS, with three biological replicates for each group. The RNA sequencing was performed by LC-BIO Biotechnology Co., Ltd. (Hangzhou, China), following a procedure that has been previously described<sup>30</sup>.

### Statistical analysis

Data processing was conducted using GraphPad Prism version 8.0.2, with all data presented as the mean ± standard mean (SM). One-way ANOVA was employed for comparisons among multiple groups, while Student's t-test or Dunnett's test was used for comparisons between two groups. All experiments were repeated at least three times. A P-value of less than 0.05 was considered to indicate a statistically significant difference.

## Results

### BPS exposure can induce renal injury in healthy rats

Our findings indicated that there was no significant difference in serum BUN or creatinine levels in rats treated with BPS compared to the control group (Fig. 1A). The research conducted by Alberto Ruiz Priego et al. demonstrated only a slight increase in renal function in mice after five weeks of treatment with 120 mg/kg b.w. of BPA, but this increase was not statistically significant<sup>22</sup>. Additionally, the study by Sebastian Mas et al. confirmed that the toxicity of BPS is lower than that of BPA. It is also noted that saturation of the metabolic and clearance pathways for BPS in rats may begin at doses of 110 mg/kg b.w. or lower. Therefore, it is understandable that exposure to BPS led to only a minor increase in BUN and SCr at the dose we selected. Furthermore, we assessed the expression of kidney injury biomarkers, specifically KIM-1 and NGAL, using immunohistochemistry. The results indicated an increased expression of KIM-1 and NGAL in the kidney tissues after BPS exposure (Fig. 1B).

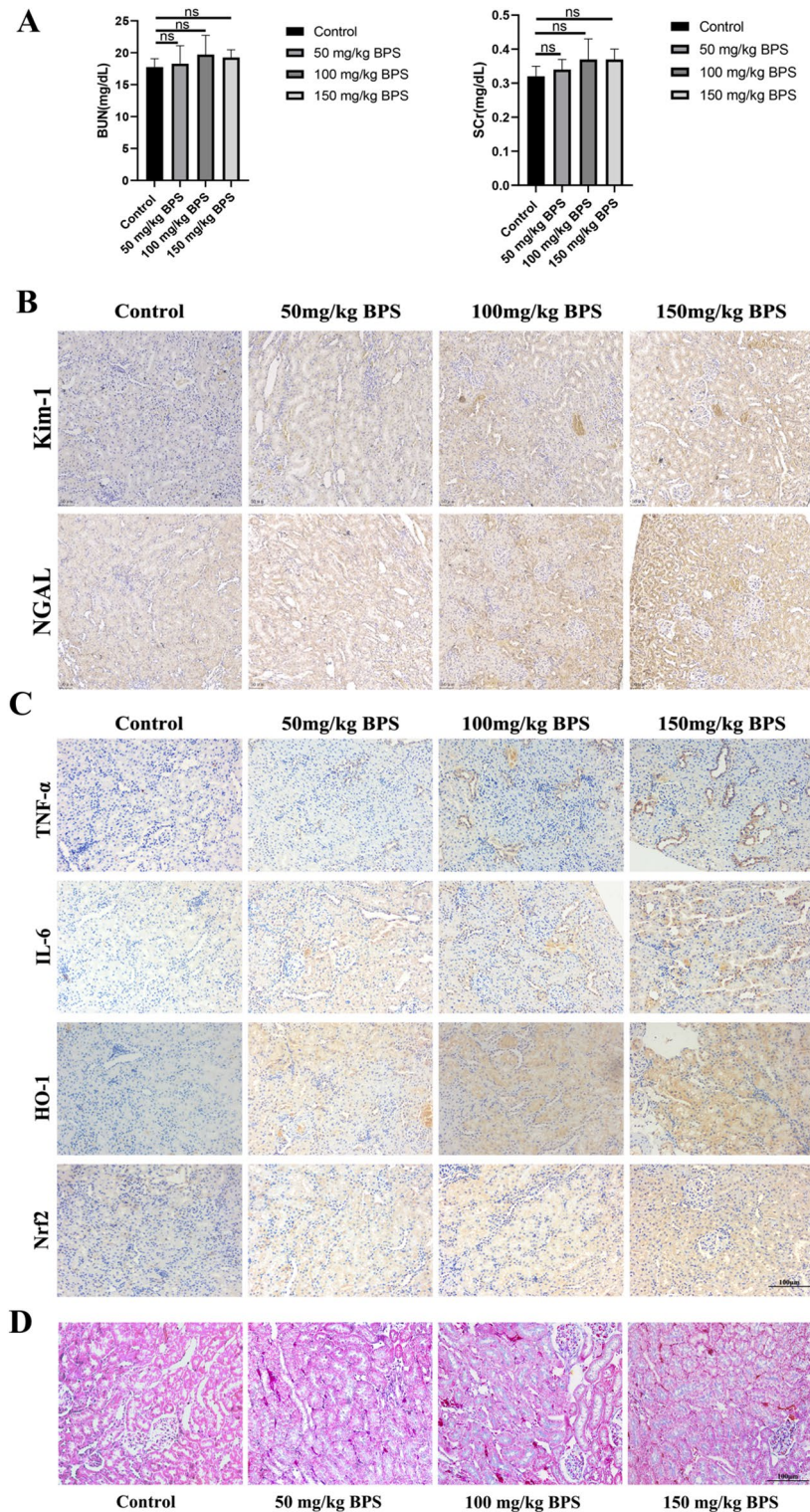


**Fig. 1.** Renal function in rats, Masson trichrome staining of kidney tissues and the expression of kidney injury related indicators after BPS exposure. **(A)** Minor increase in BUN and SCr in all rats was increased slightly after BPS treatment. ns presents no statistically significant difference compared to controls. **(B)** Immunohistochemistry showed a dose-dependent increase in Kim-1 and NGAL expression after BPS exposure. Scale bar, 50  $\mu$ m. **(C)** Immunohistochemistry showed a dose-dependent increase in TNF- $\alpha$ , IL-6, HO-1 and Nrf2 expression after BPS exposure. Scale bar, 50  $\mu$ m. **(D)** Masson trichrome staining results: the collagen fibers of the kidney tissues were significantly increased after BPS exposure, and they were concentrated around the renal tubular epithelium. Scale bar, 100  $\mu$ m.

We also measured levels of pro-inflammatory cytokines (such as IL-6 and TNF- $\alpha$ ) and oxidative stress markers (HO-1 and Nrf2) in the kidney tissue. The results showed that, compared to the control group, the expression levels of IL-6, TNF- $\alpha$ , HO-1, and Nrf2 were significantly elevated following BPS exposure (Fig. 1C). Lastly, Masson Trichrome staining revealed a significant increase in renal collagen fibers in the BPS-exposed group, with these fibers primarily concentrated around the renal tubular epithelium (Fig. 1D).

### Changes in EMT-related indicators in kidney tissues of BPS treated rats

Masson Trichrome staining demonstrated a significant increase in collagen fibers in the rat kidney following treatment with BPS. We concluded that BPS exposure resulted in fibrotic injury in the kidney. To further investigate the changes in EMT related markers in the kidney after BPS exposure, we conducted Western blot analysis. The results showed a significant reduction in the expression levels of E-cadherin and ZO-1 in renal tissue, while the expression of  $\alpha$ -SMA and vimentin increased significantly after BPS exposure (Fig. 2A). Immunofluorescence analysis revealed similar trends (Fig. 2B).

### BPS treatment affected the viability of HK-2 cells

The viability of HK-2 cells was not significantly affected at a BPS concentration of 200  $\mu$ M. However, when the concentration of BPS increased to 400  $\mu$ M, there was a significant reduction in the viability of HK-2 cells (Fig. 3A). Therefore, we chose concentrations of 100  $\mu$ M, 200  $\mu$ M, and 400  $\mu$ M for the subsequent experiments.

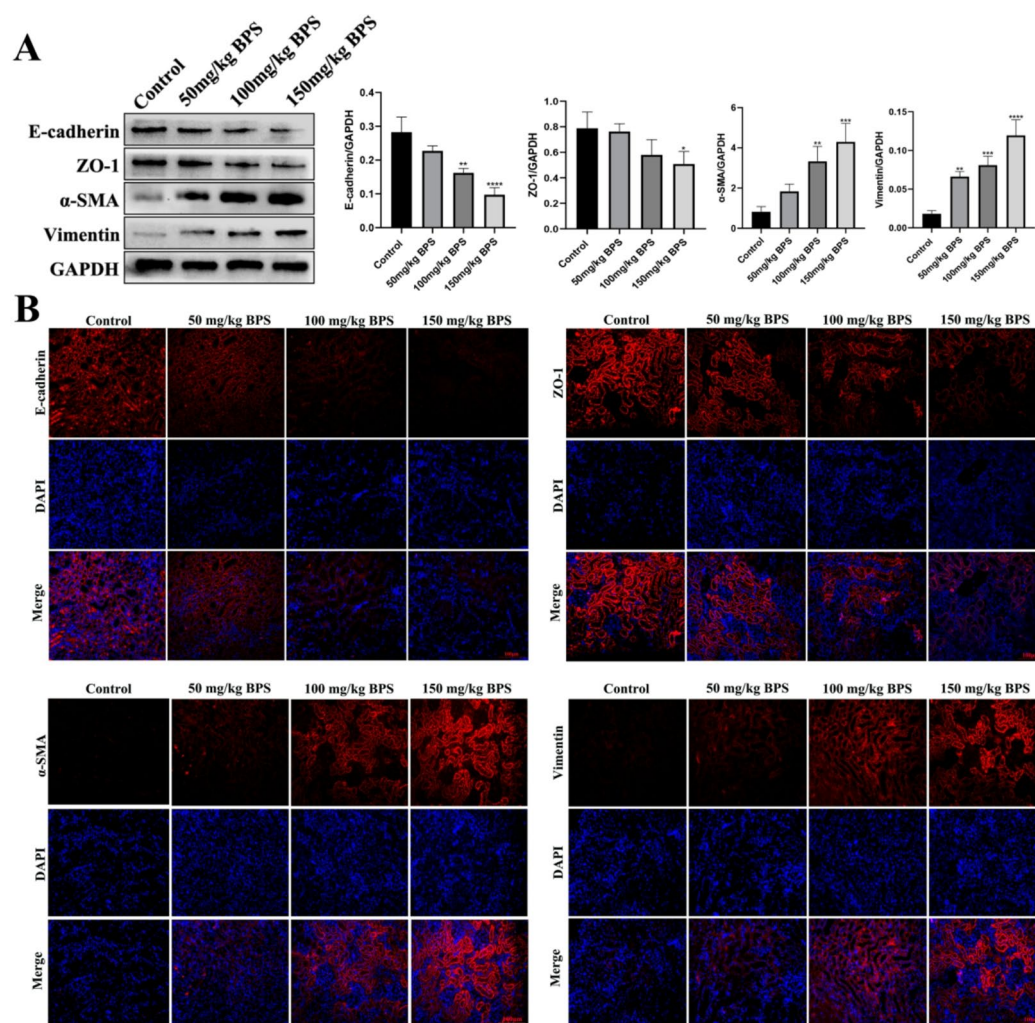


**Fig. 2.** The EMT related indicators in kidney tissues after BPS exposure. (A) Protein expression of EMT-related indicators in kidney tissue after BPS exposure. (B) Immunofluorescence images of the EMT-related indicators in kidney tissue after BPS exposure. Scale bar, 100  $\mu$ m. Data are expressed as mean  $\pm$  SD, and all the experiments were repeated three times. \* $P < 0.05$ , \*\* $P < 0.01$ , \*\*\* $P < 0.001$ , \*\*\*\* $P < 0.0001$  compared with control group.

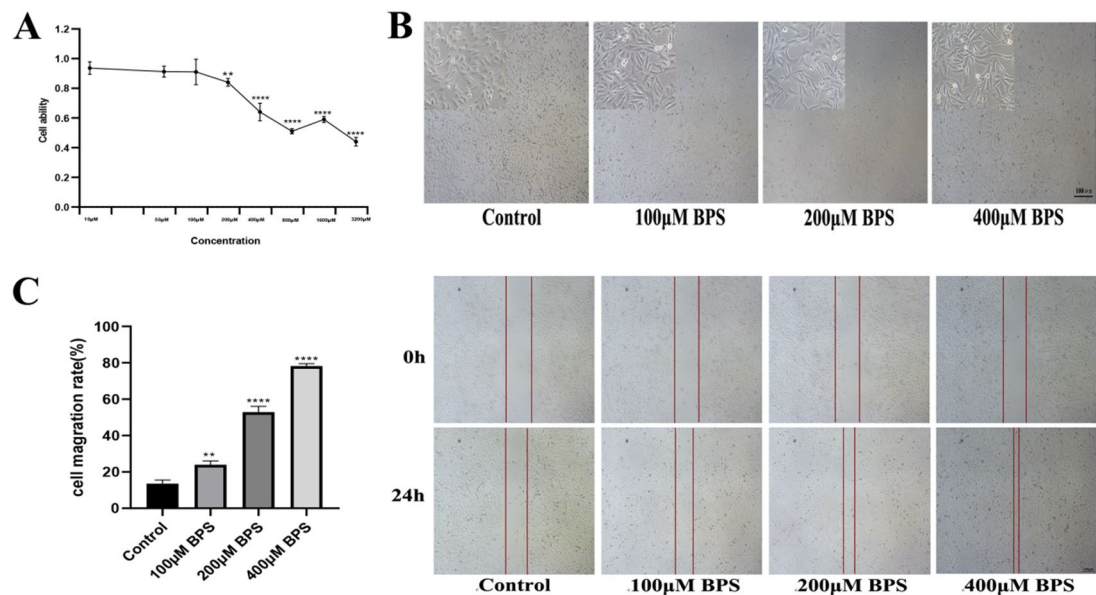


**Fig. 3.** Viability, morphology, and migration ability of HK-2 cells after BPS exposure. **(A)** HK-2 cell viability after exposure to different concentrations of BPS. **(B)** Morphological changes of HK-2 cells after BPS exposure. **(C)** Changes in the migration ability of HK-2 cells after BPS exposure. Scale bar, 100 μm. \*\* $p < 0.01$ , \*\*\*\* $p < 0.0001$  compared with 0 μM.

### BPS exposure affected cell morphology and the migration capacity of HK-2 cells

We observed that HK-2 cells morphology changed significantly after BPS exposure, the cells changed from a slightly round and plump epithelium-like morphology to a thin, irregular mesenchymal-like morphology (Fig. 3B). The results of scratch experiment showed that after 3 different doses of BPS treatment, the migration ability of HK-2 cells was significantly enhanced, and the difference was statistically significant (Fig. 3C).

### Changes in EMT-related indicators in HK-2 cells by BSP treatment

To investigate whether exposure to BPS induces EMT in HK-2 cells, we assessed the changes in markers related to epithelial and fibrosis indicators following BPS treatment. The results from western blot analysis indicated a decrease in the expression of ZO-1 and e-cadherin, along with an increase in  $\alpha$ -SMA and vimentin levels after BPS exposure (Fig. 4A). Additionally, immunofluorescence results corroborated these findings, showing consistent changes with the western blot analysis (Fig. 4B). These results suggest that EMT may have occurred in HK-2 cells exposed to BPS.

### Transcriptomic analysis of the kidney tissues and HK-2 cells after BPS exposure

To clarify the cause and mechanism of EMT in rat kidneys following exposure to BPS, we conducted RNA sequencing to identify differentially expressed genes (DEGs) in kidneys from control rats compared to those exposed to BPS. We identified a total of 795 DEGs, with 585 genes being upregulated and 210 genes downregulated (Fig. 5A). The volcano plots illustrate the distribution of these DEGs (Fig. 5B). The Gene Ontology (GO) enrichment analysis revealed that the DEGs were significantly enriched in categories related to actin filaments, cell junctions, and the regulation of PI3K activity (Fig. 5C). Additionally, the Kyoto Encyclopedia of Genes and Genomes (KEGG) analysis showed significant enrichment in the PI3K-AKT pathway (Fig. 5D). These findings suggest that the PI3K-AKT-mTOR signaling pathway may play a role in regulating renal EMT and the changes in cytoskeletal architecture induced by BPS exposure.

To clarify the causes and mechanisms of EMT changes in HK-2 cells following exposure to BPS, we conducted RNA sequencing to identify DEGs between control and BPS-exposed HK-2 cells. We identified a total of 1726 DEGs, which included 1,521 upregulated genes and 205 downregulated genes (Fig. 5E). The distribution of these DEGs is illustrated in the volcano plot (Fig. 5F). GO analysis revealed that the DEGs were primarily enriched in terms related to microtubules in the cytoskeleton and cellular components, as well as microtubule movement and microtubule binding in molecular functions. Additionally, we found enrichment in biological processes associated with microtubules and cytoskeleton regulation (Fig. 5G). KEGG analysis revealed a strong enrichment for the PI3K-AKT and MAPK signaling pathways (Fig. 5H), the specific method is based on previous studies<sup>31,32</sup>. The PI3K-AKT pathway is known to regulate mTORC1 and mTORC2, and the mTORC signaling pathway is a key pathway in regulating the cytoskeleton. Based on our RNA sequencing results from kidney tissues exposed to BPS, we hypothesize that BPS exposure may influence the cytoskeleton through the PI3K-AKT-mTOR pathway, thereby inducing EMT in HK-2 cells and contributing to renal fibrosis.

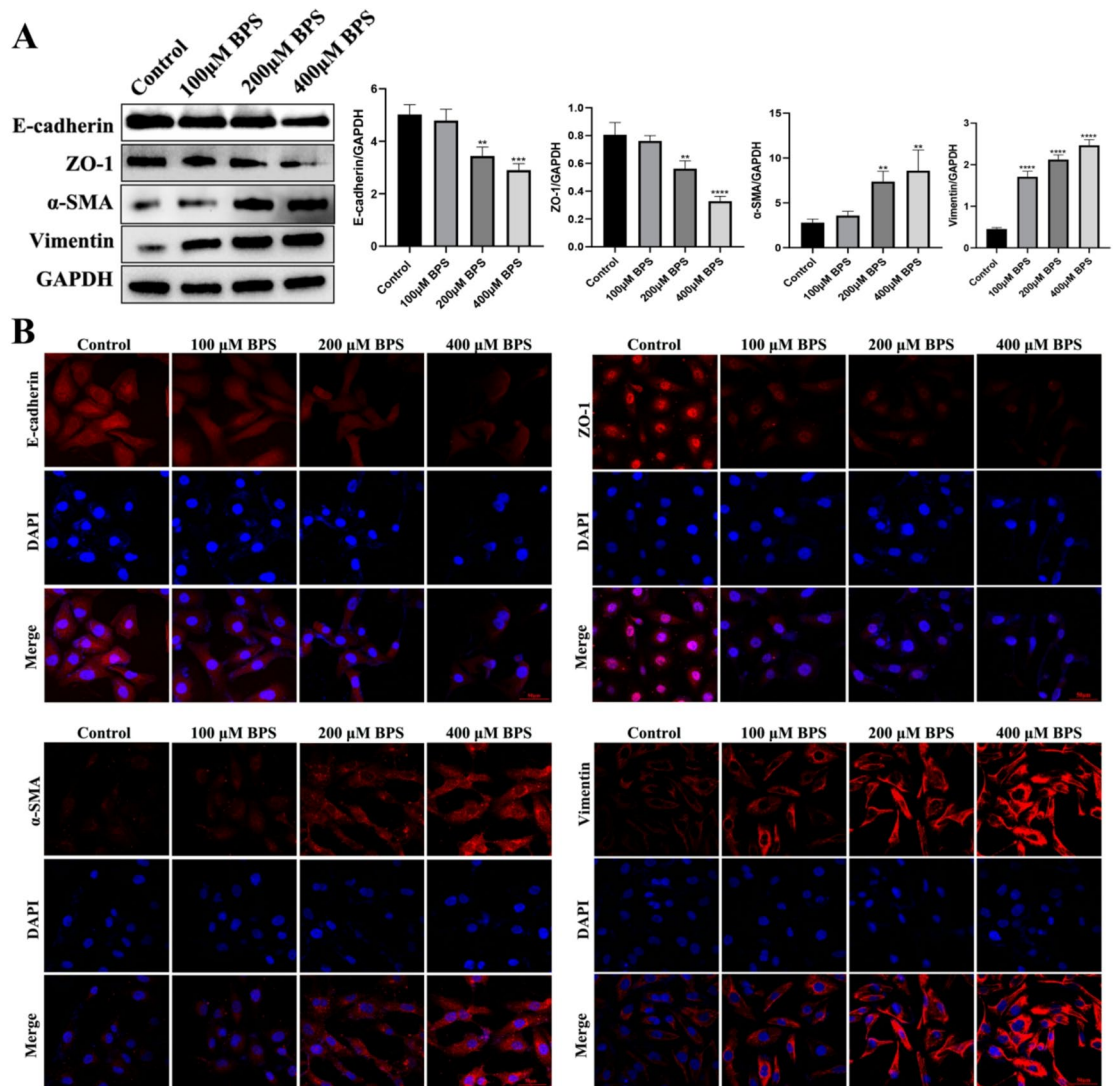


**Fig. 4.** Immunofluorescence images and protein expression of the EMT-related indicators of HK-2 cells after BPS exposure. **(A)** Protein expression of EMT-related indicators in HK-2 cells after BPS exposure. **(B)** Down-regulated expression of E-cadherin and ZO-1 in HK-2 cells after BPS exposure, and up-regulated expression of  $\alpha$ -SMA and Vimentin in HK-2 cells after BPS exposure. Scale bar, 50  $\mu$ m. Data are showed as mean  $\pm$  SD, and all experiments were repeated three times. \*\* $p < 0.01$ , \*\*\* $p < 0.001$ , \*\*\*\* $p < 0.0001$  compared with control group.

### BPS exposure activated of the PI3K-AKT-mTOR pathway and disrupted cytoskeletal architecture in HK-2 cells

The PI3K-AKT-mTOR pathway in kidney tissues and HK-2 cells were activated after BPS exposure (Fig. 6A,B). F-actin and  $\beta$ -tubulin in HK-2 cells were severely disrupted and that the cytoskeletal architecture was significantly disturbed (Fig. 6C). As we expected, the BPS activated the PI3K- AKT- mTOR pathway and disrupted the cytoskeletal architecture in HK-2 cells.

### The PI3K-AKT-mTOR signaling pathway regulates cytoskeletal architecture change and EMT in HK-2cells

To further validate the role of the PI3K-AKT-mTOR signaling pathway, we added PI3K inhibitor and mTORC inhibitor into the BPS treatment HK-2cells. We found that PI3K inhibitor significantly inhibited the activation of the level of p-PI3K, p-AKT, p-mTOR, Rictor and p-PKC (Fig. 7A), mTORC inhibitor can inhibit the levels of key proteins in the downstream pathway of mTORC, p-mTOR, Rictor and p-PKC (Fig. 8A). When the addition of PI3K inhibitor and mTORC inhibitor reduced F-actin and  $\beta$ -tubulin disruption as compared to the BPS treatment group, the changes in the cytoskeletal architecture were reversed (Figs. 7B and 8B). Meanwhile, the results of western blotting and immunofluorescence found that the PI3K inhibitor and mTORC inhibitor partially reversed the changes in the EMT-related indicators induced by BPS treatment (Figs. 7C,D and 8C). The above results suggest that the cytoskeletal architecture change and EMT induced by BPS exposure are indeed regulated by the PI3K-AKT-mTOR signaling pathway.

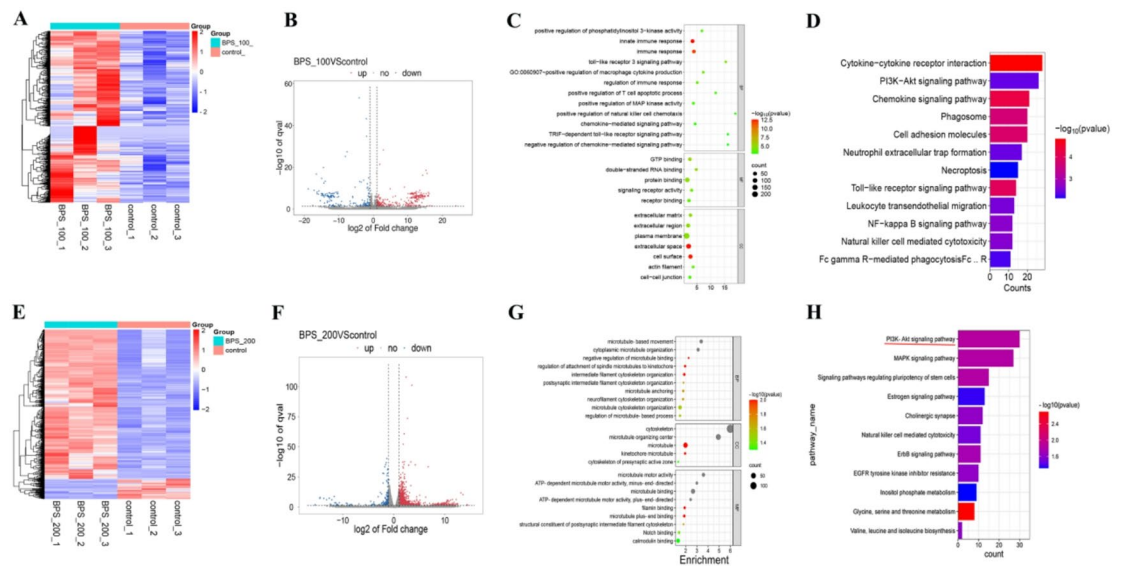


**Fig. 5.** RNA sequencing of kidney tissues and HK-2 cells in the control and BPS exposed groups. **(A)** Heatmap of DEGs of kidney tissues. **(B)** Volcano plots of DEGs of kidney tissues. **(C)** GO enrichment analysis of DEGs of kidney tissues. **(D)** KEGG enrichment analysis of DEGs of kidney tissues. **(E)** Heatmap of DEGs of HK-2 cells. **(F)** Volcano plots of DEGs of HK-2 cells. **(G)** GO enrichment analysis of DEGs of HK-2 cells. **(H)** KEGG enrichment analysis of DEGs of HK-2 cells. The KEGG enrichment analysis was taken from the relevant website: [www.kegg.jp/kegg/kegg1.html](http://www.kegg.jp/kegg/kegg1.html).

## Discussion

There is an ongoing debate regarding the toxicity of BPS as a substitute for BPA. Recent studies have indicated that BPS can damage multiple systems in the body, including the reproductive system, liver, brain, and cardiovascular system<sup>33</sup>. Specifically, BPS has been found to harm the testis, leading to altered endocrine function in the male reproductive system. A population-based epidemiological study has shown that long-term prenatal exposure to BPS and BPA negatively affects neurodevelopment in children, particularly in boys<sup>34</sup>. Additionally, prolonged exposure to BPA-like compounds can induce anxiety and depressive behaviors, increase gut permeability, and enhance microbial diversity<sup>35</sup>. Research has demonstrated that subchronic exposure to BPS can lead to liver damage in mice due to oxidative stress<sup>36</sup>. At environmentally relevant concentrations, BPS has shown significant and irreversible effects on the basic communication functions of neurons in the mature vertebrate brain<sup>37</sup>. Furthermore, BPS exposure has been linked to the acceleration of atherosclerosis, developmental malformations, and abnormal behavior<sup>38–40</sup>. Due to its estrogenic effects, BPS may also increase the risk of breast cancer, even at doses lower than what the U.S. Food and Drug Administration (FDA) deems safe for consumption<sup>41</sup>. However, there are limited studies addressing the impact of BPS on renal injury. Research by Feng et al. showed that when treating adrenocortical cancer cell lines with BPA and BPS, BPS was less toxic than BPA<sup>42</sup>. Similarly, a study by Sebastian Mas et al. found that BPS exhibited lower toxicity to HK-2 cells compared to BPA<sup>43</sup>. Although evidence suggests that BPS exposure can lead to significant nephrotoxicity, the extent of kidney damage caused by BPS and its underlying mechanisms remain poorly understood<sup>44,45</sup>. This study aims to investigate the specific phenotype and potential mechanisms involved in kidney injury resulting from BPS exposure through both in vivo and in vitro experiments.

According to reports, the average American adult consumes approximately 1.31 ng/kg of BPS per day. Additionally, data from animal and human exposure between 2007 and 2013 indicate that BPA doses below 50 mg/kg b.w. /day can affect female reproduction and may also have negative implications for male reproductive health<sup>46</sup>. Currently, there is no definitive data on the dose of BPA in humans that would lead to significant kidney damage. A previous study indicated that the metabolic saturation concentration of BPS in rats is 110 mg/kg b.w.<sup>27</sup>. Therefore, we selected doses of 50 mg/kg b.w., 100 mg/kg b.w., and 150 mg/kg b.w. of BPS, which align with previous intervention concentrations of BPA associated with kidney injury<sup>47</sup>. NGAL and KIM-1 are recognized markers of kidney injury. A clinical study demonstrated that urinary BPA concentrations were positively correlated with increased levels of NGAL and KIM-1<sup>48</sup>. Furthermore, research by Priego et al. found that five weeks of BPA exposure resulted in heightened expression of NGAL and KIM-1 in kidney tissue<sup>22</sup>. Our study also confirmed that five weeks of BPS exposure increased the NGAL and KIM-1 indices, indicating that BPS exposure leads to renal tubular injury. Additionally, we observed fiber deposition in the tubular epithelium as a result of BPS exposure.

The ultimate common pathway and histological manifestation of CKD is renal fibrosis, and multiple etiologies can lead to renal fibrosis. In recent years, kidney damage caused by environmental pollutants has gradually attracted attention. For example, prolonged exposure to PM2.5 increases the prevalence of CKD<sup>49</sup>; DEHP causes EMT in the renal tubules, thus aggravating renal fibrosis and renal disease<sup>50</sup>. However, fibrogenesis features include increased matrix production and decreased degradation, matrix receptor regulation promoting cell-

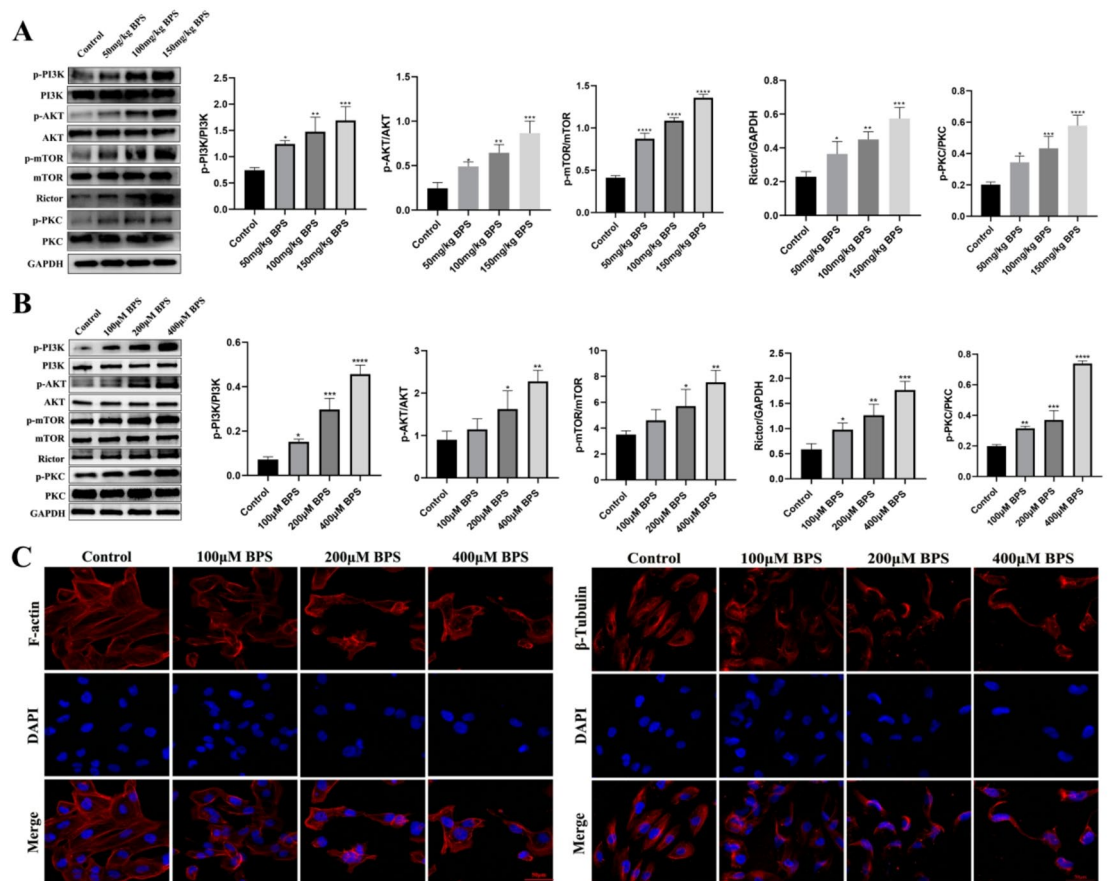


**Fig. 6.** Changes of the PI3K-AKT-mTOR pathway and the cytoskeletal architecture in kidney tissues and HK-2 cells after BPS exposure. **(A)** Protein expression of PI3K-AKT-mTOR pathway in kidney tissues after BPS exposure, data are shown as mean  $\pm$  standard deviation, and all experiments were repeated three times.  $^*p < 0.05$ ,  $^{**}p < 0.01$ ,  $^{***}p < 0.001$ ,  $^{****}p < 0.0001$  compared with control group. **(B)** Protein expression of PI3K-AKT-mTOR pathway in HK-2 cells after BPS exposure, data are shown as mean  $\pm$  standard deviation, and all experiments were repeated three times.  $^{**}p < 0.01$ ,  $^{***}p < 0.001$ ,  $^{****}p < 0.0001$  compared with control group. **(C)** Immunofluorescence image of the HK-2 cytoskeletal architecture after BPS exposure. F-actin and  $\beta$ -Tubulin were extensively disrupted in HK-2 cells after BPS treatment. Scale bar, 50  $\mu$ m.

matrix interactions, and EMT, etc<sup>51,52</sup>. The renal tubular epithelial cells due to cell death and dedifferentiation, lead to changes in characteristic EMT markers, and ultimately, and ultimately lead to the occurrence of EMT. During EMT, epithelial cell adhesion is reduced and motility is enhanced. The loss of epithelial cell markers is also involved in the process of EMT. For example, the expression of E-cadherin and the occlusive band (ZO-1) decrease<sup>53</sup>. E-cadherins bind to adjacent cells to form an epithelial barrier and establish a bridge between the cytoskeleton of adjacent cells<sup>54</sup>. ZO-1 is the structural basis for regulating cytoskeletal organization and polarity<sup>55,56</sup>. The EMT process also includes the upregulation of  $\alpha$ -SMA and vimentin, intermediate filaments that reduce the transport of E-cadherin to the cell surface<sup>57</sup> and the development of the mesenchymal phenotype by acquiring mesenchymal markers and abilities<sup>58</sup>.  $\alpha$ -SMA is also one of the typical mesenchymal markers<sup>59</sup>. Our research found EMT in kidney after BPS exposure, and it is mainly focused on the tubular epithelial.

The essence of EMT is the remodeling of the cytoskeleton, and the sequencing data from in vivo and in vitro experiments in this study are highly enriched to the cytoskeleton. The cytoskeleton is fundamental to the maintenance of cell morphology and motility, organizing the cytoplasm and building the spindle bodies<sup>60</sup>. F-actin are an important part of the cytoskeleton. The dynamic remodeling of these protein filaments provides the power for cell invasion and migration, and changes in actin structure in cells are closely related to EMT<sup>61</sup>. The actin cytoskeleton is a continuously reconstructed, dynamic structure that is maintained by the well-balanced, local assembly, and disassembly of actin filaments<sup>62</sup>. Microtubule non-covalent polymers form part of the cytoskeleton, and the microtubules are highly complex and composed mainly of heterodimeric  $\alpha$ -tubulin and  $\beta$ -tubulin, and functionalized through various evolutionarily conserved posttranslational modifications<sup>63</sup>. Microtubules have a dynamic instability and can spontaneously polymerize and depolymerize<sup>64</sup>. It was shown that exposure to the environmental contaminant PS-MPs can truncate actin filaments to disrupt the cytoskeleton, leading to the disruption of the BTB integrity<sup>65</sup>. BPS also induced truncation of microtubules and actin filaments in the testis<sup>26</sup>. We confirmed that BPS exposure induces EMT in HK-2 cells and kidney tissues, and that the cytoskeletal architecture is a key driver of EMT. To verify whether BPS exposure induces cytoskeletal

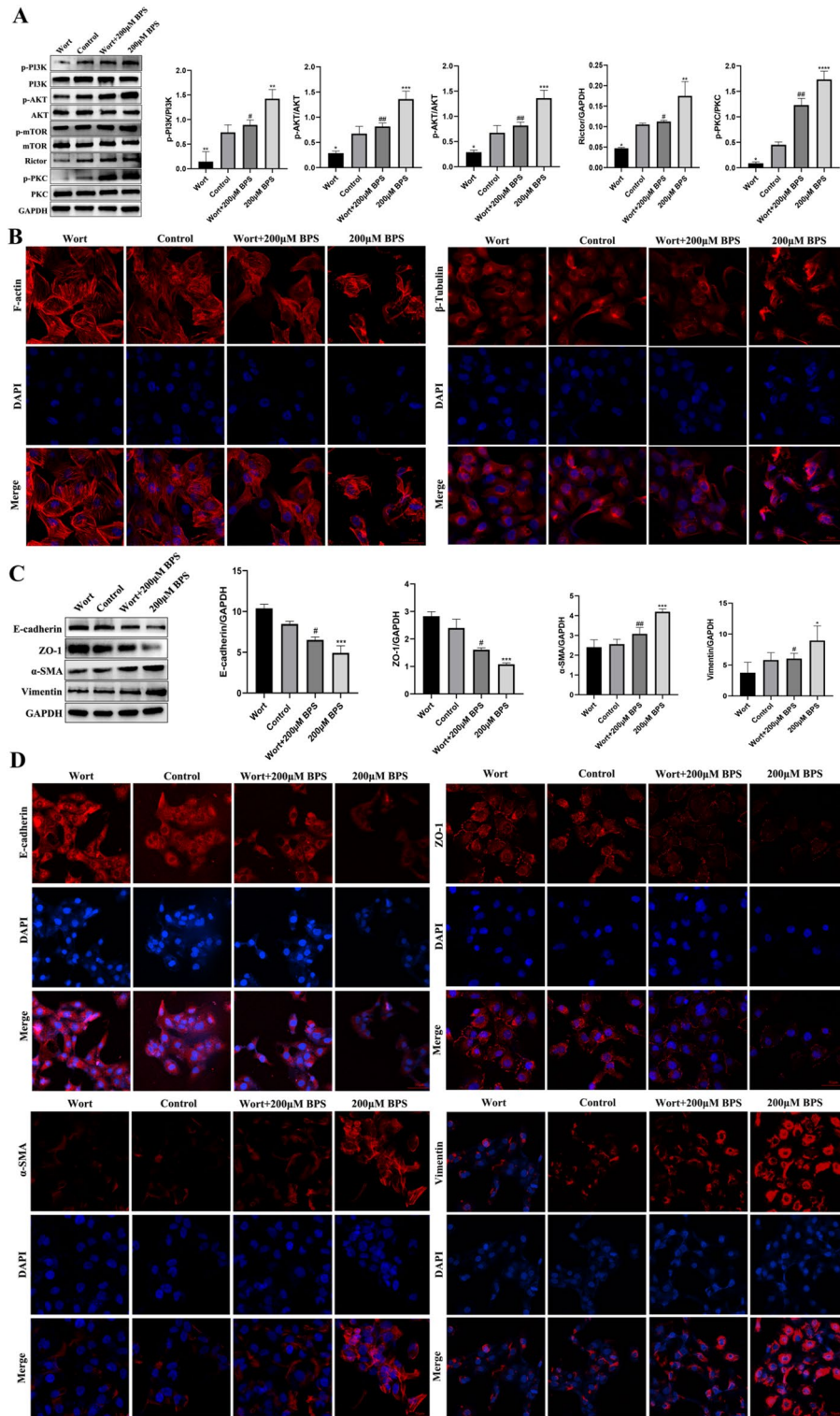


**Fig. 7.** Changes of the PI3K-AKT-mTOR pathway, cytoskeletal architecture, and EMT-related indicators after the administration of the PI3K inhibitor wortmannin(Wort). **(A)** Protein expression associated with the PI3K-AKT-mTOR pathway after treatment with BPS and PI3K inhibitor. Data are showed as mean ± SD, and all experiments were repeated at least three times. \*\* $p < 0.01$ , \*\*\* $p < 0.001$  and \*\*\*\* $p < 0.0001$  compared with control group. # $p < 0.05$  and ## $p < 0.01$  compared to the 200 µM BPS group. **(B)** Immunofluorescence detection of cytoskeletal architecture changes after BPS and PI3K inhibitor treatment. Scale bar, 50 µm. **(C)** Expression of EMT-related proteins after BPS and PI3K inhibitor treatment.\* $p < 0.05$  and \*\*\* $p < 0.001$  compared with control group. # $p < 0.05$  and ## $p < 0.01$  compared to the 200 µM BPS group. **(D)** Immunofluorescence images of EMT-related indicators in HK-2 cells after BPS and PI3K inhibitor treatment. Scale bar, 50 µm. Data are showed as mean ± SD, and all experiments were repeated three times.

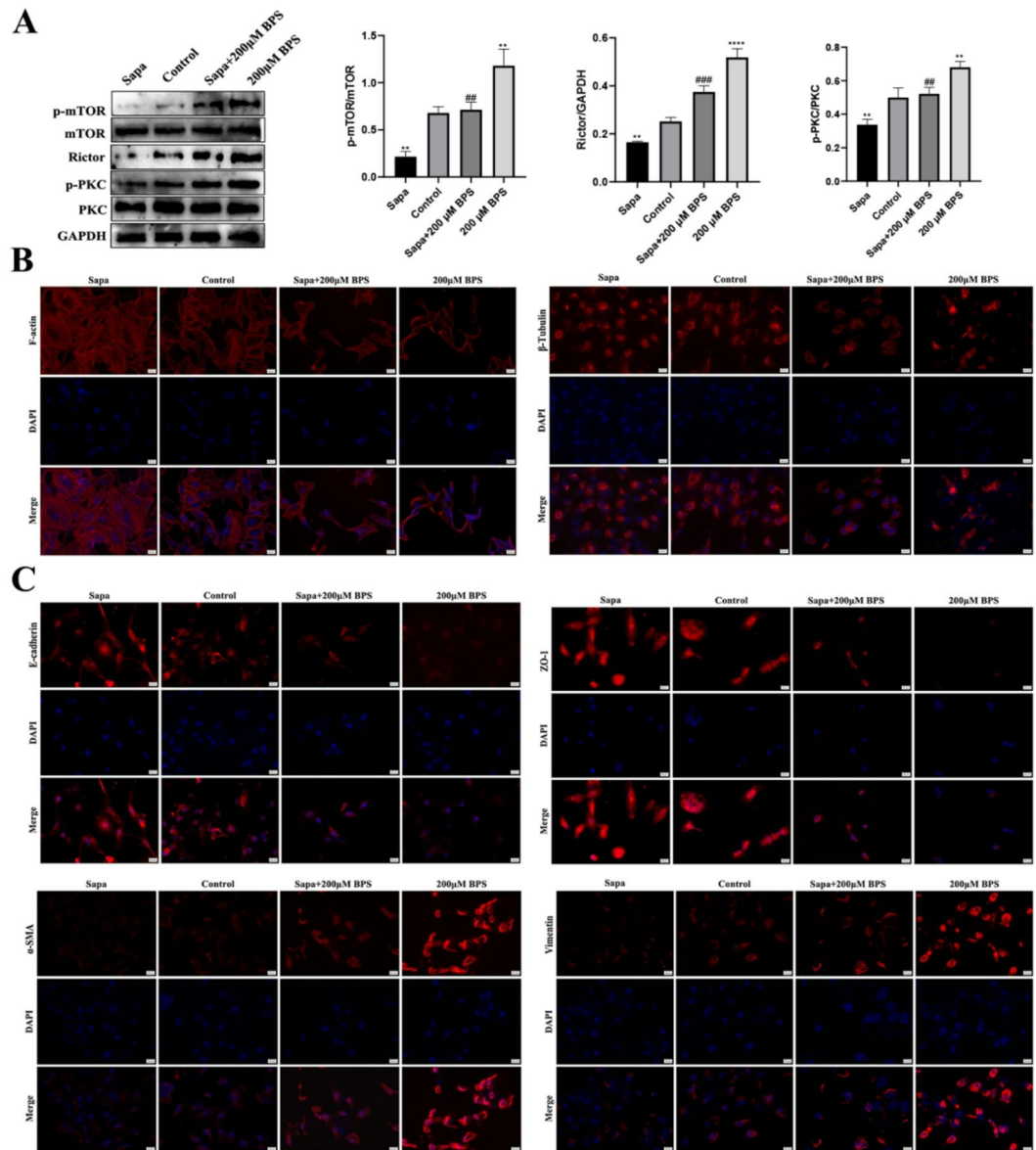


**Fig. 8.** Changes of the mTOR pathway, cytoskeletal architecture, and EMT-related indicators after the administration of the mTORC inhibitor Sapanisertib(Sapa). (A) Protein expression associated with the mTOR pathway after treatment with BPS and mTORC inhibitor. Data are showed as mean  $\pm$  SD, and all experiments were repeated at least three times.  $**p < 0.01$ ,  $***p < 0.001$  and  $****p < 0.0001$  compared with control group.  $\#p < 0.05$  and  $\##p < 0.01$  compared to the 200  $\mu$ M BPS group. (B) Immunofluorescence detection of cytoskeletal architecture changes after BPS and mTORC inhibitor treatment. Scale bar, 20  $\mu$ m. (C) Immunofluorescence images of EMT-related indicators in HK-2 cells after BPS and mTORC inhibitor treatment. Scale bar, 20  $\mu$ m. Data are showed as mean  $\pm$  SD, and all experiments were repeated three times.

architecture changes in HK-2, we further examined the changes in cytoskeletal architecture F-actin and  $\beta$ -Tubulin after BPS exposure by immunofluorescence, and we found that BPS exposure indeed induced changes in HK-2 cytoskeletal architecture.

Many pathways can control EMT and cytoskeletal architecture. The study by Zhang et al. found that knockdown of WNT5A significantly inhibited BPS-induced HK-2 cell migration, and disrupted the EMT process<sup>66</sup>. The sequencing results in our study suggest that differential genes after BPS exposure are highly enriched in the PI3K-AKT signaling pathway. The study of Yang et al. explored the relationship between WNT5A and PI3K-AKT signaling pathway, constructed cells overexpressing WNT5A, and found that the phosphorylation level of PI3K and AKT was significantly increased after overexpression of WNT5A by sequencing. In addition, the expression level of WNT5A could be reversed by using PI3K inhibitors<sup>67</sup>. Triptolide can reverse EMT in HK-2 cells by reducing PI3K-AKT signaling activity<sup>68</sup>. The PI3K-AKT pathway can be regulated by Nrf2-HO-1-mediated ROS and regulate the high glucose-induced EMT in HK-2 cells<sup>69</sup>. This study also found that the expression level of Nrf2 and HO-1 in renal tissue was significantly increased after BPS induction. Moreover, EMT by hdc

5-mediated treatment in renal tubular cells of diabetic nephropathy can be affected by PI3K-AKT pathway, while *mettl14*-mediated PTEN could regulate the activity of PI3K-AKT pathway<sup>70</sup>. These results indicate that the PI3K-AKT pathway can regulate the EMT process in renal tubular epithelial cells and regulate downstream mTORC1 and mTORC2 expression. The mTOR interacts with Raptor and Rictor to form the mTORC1 and mTORC2, respectively<sup>71</sup>. Substantial evidence suggests that abnormal activation of mTORC1 may be associated in kidney disease, and mTORC1 plays an important role in high glucose-induced EMT and diabetes-induced renal fibrosis in HK-2 cells<sup>72</sup>; mTORC1 also plays a key role in the nephrotoxic effects of FB1, and fumarylacetoacetate (FB1) is a global polluting mycotoxin that is closely associated with unexplained CKD<sup>73</sup>. However, mTORC2 in kidney disease is less studied and controversial. It has been shown that the Rictor / mTORC2 pathway regulates TGF  $\beta$  1-induced renal fibroblast activation<sup>74</sup>. However, it has also been shown that endogenous Rictor/mTORC2 prevents cisplatin-induced acute kidney injury<sup>75</sup>. mTORC1 and mTORC2 have also been confirmed to regulate the cytoskeletal architecture. mTORC2 can regulate osteoblast differentiation by regulating cytoskeletal architecture reorganization<sup>76</sup>, and phosphorylation of the actin cytoskeletal architecture can be regulated by the Rictor /TOR complex<sup>77</sup>. mTORC1 pathway activation can promote actin cytoskeletal architecture, thereby promoting IGF-1-induced cancer cell migration and invasion<sup>78</sup>. The above studies indicate that the PI3K-AKT-mTOR pathway and cytoskeletal architecture rearrangements play an important role in EMT. The result of RNA sequencing found that DEGs after BPS exposure were enriched in the PI3K-AKT signaling pathway and cytoskeleton. The key proteins associated with PI3K-AKT-mTOR pathway were detected and the results showed that BPS exposure activated the PI3K-AKT-mTOR pathway. In addition, we inhibited the pathway with a PI3K inhibitor, and further observed cytoskeletal architecture changes and EMT, which found that the cytoskeletal architecture alterations and EMT caused by BPS exposure were partially reversed by PI3K inhibitor. Our study showed that BPS exposure mediated EMT and changes in HK-2 cytoskeletal structures through PI3K-AKT-mTOR signaling and that PI3K inhibitor partially reversed HK-2 cytoskeletal disorders and EMT.

## Conclusions

Taken together, our results suggest that BPS exposure can induce renal fibrosis injury, while EMT and HK-2 cytoskeletal architecture alteration play a key role in renal fibrosis damage induced by BPS exposure, and PI3K-AKT-mTOR signaling pathway may regulate cytoskeletal architecture changes and EMT. To the best of our knowledge, our study is the first to investigate the phenotype and specific mechanism of kidney injury induced by BPS exposure in a combination of in vivo in vitro assay as well as transcriptomic analysis. This study is essential for BPS or other environmental pollutants and subsequent clinical treatment of kidney damage.

## Data availability

The datasets used or analyzed during the current study are available from the corresponding author on reasonable request.

Received: 9 January 2025; Accepted: 21 November 2025

Published online: 05 December 2025

## References

- Lehmler, H. J., Liu, B., Gadogbe, M. & Bao, W. Exposure to bisphenol A, bisphenol F, and bisphenol S in U.S. adults and children: The National Health and Nutrition Examination Survey 2013–2014. *ACS Omega* **3**(6), 6523–6532. <https://doi.org/10.1021/acscomega.8b00824> (2018).
- Sola, C. et al. Spoligotype database of *Mycobacterium tuberculosis*: biogeographic distribution of shared types and epidemiologic and phylogenetic perspectives. *Emerg. Infect. Dis.* **7**(3), 390–396. <https://doi.org/10.3201/eid0703.010304> (2001).
- Huang, Y. Q. et al. A (BPA) in China: A review of sources, environmental levels, and potential human health impacts. *Environ. Int.* **42**, 91–99. <https://doi.org/10.1016/j.envint.2011.04.010> (2012).
- Wei, Y. et al. Maternal exposure to bisphenol A during pregnancy interferes ovaries development of F1 female mice. *Theriogenology* **142**, 138–148. <https://doi.org/10.1016/j.theriogenology.2019.09.045> (2020).
- Zhang, Y. F. et al. A alternatives bisphenol S and bisphenol F interfere with thyroid hormone signaling pathway in vitro and in vivo. *Environ. Pollut.* **237**, 1072–1079. <https://doi.org/10.1016/j.envpol.2017.11.027> (2018).
- Zhang, Y. F. et al. Cardiovascular toxicity and mechanism of bisphenol A and emerging risk of bisphenol S. *Sci. Total Environ.* **723**, 137952. <https://doi.org/10.1016/j.scitotenv.2020.137952> (2020).
- Liao, C. & Kannan, K. Profiles of bisphenol A and other bisphenol analogues in foodstuffs from the United States and their implications for human exposure. *J. Agric. Food Chem.* **61**(19), 4655–4662. <https://doi.org/10.1021/jf400445n> (2013).
- ECHA. *Market survey: Use of bisphenol A and its alternatives in thermal paper in the EU from 2014 to 2017*. Available from: [https://echa.europa.eu/documents/10162/22863068/bpa\\_in\\_thermal\\_paper\\_report\\_en.pdf/0d93cd76-345e-2ed4-698f-a3beae6d755](https://echa.europa.eu/documents/10162/22863068/bpa_in_thermal_paper_report_en.pdf/0d93cd76-345e-2ed4-698f-a3beae6d755) (2018).
- Guo, H. et al. Structural benefits of bisphenol S and its analogs resulting in their high sorption on carbon nanotubes and graphite. *Environ. Sci. Pollut. Res. Int.* **23**(9), 8976–8984. <https://doi.org/10.1007/s11356-016-6040-7> (2016).
- Danzl, E., Sei, K., Soda, S., Ike, M. & Fujita, M. Biodegradation of bisphenol A, bisphenol F and bisphenol S in seawater. *Int. J. Environ. Res. Public Health.* **6**(4), 1472–1484. <https://doi.org/10.3390/ijerph6041472> (2009).
- Zhang, B. et al. Concentrations of bisphenol A and its alternatives in paired maternal-fetal urine, serum and amniotic fluid from an e-waste dismantling area in China. *Environ. Int.* **136**, 105407. <https://doi.org/10.1016/j.envint.2019.105407> (2020).
- Collins, A. J. et al. US renal data system 2013 annual data report. *Am. J. Kidney Dis.*, **63**(1 Suppl), A7. <https://doi.org/10.1053/j.ajkd.2013.11.001>. (2014).
- Friedman, S. L., Sheppard, D., Duffield, J. S. & Violette, S. Therapy for fibrotic diseases: Nearing the starting line. *Sci. Transl. Med.* **5**(167), 167sr1. <https://doi.org/10.1126/scitranslmed.3004700> (2013).
- Kramann, R., Wongboonsin, J., Chang-Panesso, M., Machado, F. G. & Humphreys, B. D. Gli1(+) pericyte loss induces capillary rarefaction and proximal tubular injury. *J. Am. Soc. Nephrol.* **28**(3), 776–784. <https://doi.org/10.1681/ASN.2016030297> (2017).
- Gokmen, M. R. & Lord, G. M. Aristolochic acid nephropathy. *BMJ* **344**, e4000. <https://doi.org/10.1136/bmj.e4000> (2012).

16. Li, D. et al. Exosomes from human umbilical cord mesenchymal stem cells reduce damage from oxidative stress and the epithelial-mesenchymal transition in renal epithelial cells exposed to oxalate and calcium oxalate monohydrate. *Stem Cells Int.* **2019**, 6935806. <https://doi.org/10.1155/2019/6935806> (2019).
17. Chevalier, R. L., Forbes, M. S. & Thornhill, B. A. Ureteral obstruction as a model of renal interstitial fibrosis and obstructive nephropathy. *Kidney Int.* **75**(11), 1145–1152. <https://doi.org/10.1038/ki.2009.86> (2009).
18. Aranda-Rivera, A. K., Cruz-Gregorio, A., Aparicio-Trejo, O. E., Ortega-Lozano, A. J. & Pedraza-Chaverri, J. Redox signaling pathways in unilateral ureteral obstruction (UUO)-induced renal fibrosis. *Free Radic Biol. Med.* **172**, 65–81. <https://doi.org/10.1016/j.freeradbiomed.2021.05.034> (2021).
19. Dongre, A. Weinberg. New insights into the mechanisms of epithelial-mesenchymal transition and implications for cancer. *Nat. Rev. Mol. Cell. Biol.* **20**(2), 69–84. <https://doi.org/10.1038/s41580-018-0080-4> (2019).
20. Lamouille, S. & Derynck, R. Cell size and invasion in TGF-beta-induced epithelial to mesenchymal transition is regulated by activation of the mTOR pathway. *J. Cell. Biol.* **178**(3), 437–451. <https://doi.org/10.1083/jcb.200611146> (2007).
21. Bakin, A. V., Tomlinson, A. K., Bhowmick, N. A., Moses, H. L. & Artega, C. L. Phosphatidylinositol 3-kinase function is required for transforming growth factor beta-mediated epithelial to mesenchymal transition and cell migration. *J. Biol. Chem.* **275**(47), 36803–36810. <https://doi.org/10.1074/jbc.M005912200> (2000).
22. Priego, A. R., Parra, E. G., Mas, S., Morgado-Pascual, J. L., Ruiz-Ortega, M. & Rayego-Mateos, S. Bisphenol A modulates autophagy and exacerbates chronic kidney damage in mice. *Int. J. Mol. Sci.* **22**(13), 7189. <https://doi.org/10.3390/ijms22137189> (2021).
23. Bosch-Panadero, E. et al. Bisphenol A is an exogenous toxin that promotes mitochondrial injury and death in tubular cells. *Environ. Toxicol.* **33**(3), 325–332. <https://doi.org/10.1002/tox.22519> (2018).
24. Mandrah, K. et al. A study on bisphenol S induced nephrotoxicity and assessment of altered downstream kidney metabolites using gas chromatography-mass spectrometry based metabolomics. *Environ. Toxicol. Pharmacol.* **93**, 103883. <https://doi.org/10.1016/j.eap.2022.103883> (2022).
25. Shen, Y. et al. A analogs in patients with chronic kidney disease and dialysis therapy. *Ecotoxicol. Environ. Saf.* **185**, 109684. <https://doi.org/10.1016/j.ecoenv.2019.109684> (2019).
26. Wu, H. et al. Bisphenol S perturbs Sertoli cell junctions in male rats via alterations in cytoskeletal organization mediated by an imbalance between mTORC1 and mTORC2. *Sci. Total Environ.* **762**, 144059. <https://doi.org/10.1016/j.scitotenv.2020.144059> (2021).
27. Waidyanatha, S. et al. Comparative toxicokinetics of bisphenol S in rats and mice following Gavage administration. *Toxicol. Appl. Pharmacol.* **406**, 115207. <https://doi.org/10.1016/j.taap.2020.115207> (2020).
28. Zhanghuang, C. et al. Doxycycline hydrochloride regulates cytoskeletal rearrangement and epithelial-to-mesenchymal transition in malignant rhabdoid tumour of the kidney. *Biomed. Res. Int.* **2022**, 2760744. <https://doi.org/10.1155/2022/2760744> (2022).
29. Zhang, Z. et al. Comprehensive proteomic analysis of exosome mimetic vesicles and exosomes derived from human umbilical cord mesenchymal stem cells. *Stem Cell. Res. Ther.* **13**(1), 312. <https://doi.org/10.1186/s13287-022-03008-6> (2022).
30. Wang, J. et al. Multiple transcriptomic profiling: p53 signaling pathway is involved in DEHP-induced prepubertal testicular injury via promoting cell apoptosis and inhibiting cell proliferation of Leydig cells. *J. Hazard. Mater.* **406**, 124316. <https://doi.org/10.1016/j.jhazmat.2020.124316> (2021).
31. Kanehisa, O., Sato, M., Kawashima, Y., Furumichi, M. & Tanabe M. KEGG as a reference resource for gene and protein annotation. *Nucleic Acids Res.* **44**(D1), D457–D462. <https://doi.org/10.1093/nar/gkv1070> (2016).
32. Kanehisa, M. & Goto, S. K. E. G. G. Kyoto encyclopedia of genes and genomes. *Nucleic Acids Res.* **28**(1), 27–30. <https://doi.org/10.1093/nar/28.1.27> (2000).
33. Ullah, A. et al. Bisphenol A and its analogs bisphenol B, bisphenol F, and bisphenol S: Comparative in vitro and in vivo studies on the sperms and testicular tissues of rats. *Chemosphere* **209**, 508–516. <https://doi.org/10.1016/j.chemosphere.2018.06.089> (2018).
34. Jiang, Y. et al. Prenatal exposure to bisphenol A and its alternatives and child neurodevelopment at 2 years. *J Hazard. Mater.* **388**, 121774. <https://doi.org/10.1016/j.jhazmat.2019.121774> (2020).
35. Singh, D. P. et al. Sexual dimorphism in neurobehavioural phenotype and gut microbial composition upon long-term exposure to structural analogues of bisphenol-A. *J. Hazard. Mater.* **476**, 135178. <https://doi.org/10.1016/j.jhazmat.2024.135178> (2024).
36. Zhang, Z. et al. Bisphenol S exposure affects liver function in mice involving oxidative damage. *Regul. Toxicol. Pharmacol.* **92**, 138–144. <https://doi.org/10.1016/j.yrtph.2017.11.018> (2018).
37. Schirmer, E., Schuster, S. & Machnik, P. Bisphenols exert detrimental effects on neuronal signaling in mature vertebrate brains. *Commun. Biol.* **4**(1), 465. <https://doi.org/10.1038/s42003-021-01966-w> (2021).
38. Wang, W. et al. Bisphenol S exposure accelerates the progression of atherosclerosis in zebrafish embryo-larvae. *J. Hazard. Mater.* **426**, 128042. <https://doi.org/10.1016/j.jhazmat.2021.128042> (2022).
39. Saïli, K. S. et al. Neurodevelopmental low-dose bisphenol A exposure leads to early life-stage hyperactivity and learning deficits in adult zebrafish. *Toxicology* **291**(1–3), 83–92. <https://doi.org/10.1016/j.tox.2011.11.001> (2012).
40. Kim, S. S. et al., Neurochemical and behavioral analysis by acute exposure to bisphenol A in zebrafish larvae model. *Chemosphere* **239**, 124751. <https://doi.org/10.1016/j.chemosphere.2019.124751> (2020).
41. Stillwater, B. J., Bull, A. C., Romagnolo, D. F., Neumayer, L. A., Donovan, M. G. & Selmin, O. I. Bisphenols and risk of breast cancer: A narrative review of the impact of diet and bioactive food components. *Front. Nutr.* **7**, 581388. <https://doi.org/10.3389/fnut.2020.581388> (2020).
42. Feng, Y. et al. Effects of bisphenol analogues on steroidogenic gene expression and hormone synthesis in H295R cells. *Chemosphere* **147**, 9–19. <https://doi.org/10.1016/j.chemosphere.2015.12.081> (2016).
43. Mas, S. et al. Bisphenol S is a haemodialysis-associated xenobiotic that is less toxic than bisphenol A. *Clin. Kidney J.* **14**(4), 1147–1155. <https://doi.org/10.1093/ckj/sfaa071> (2021).
44. Zhao, C. et al. MALDI-MS imaging reveals asymmetric spatial distribution of lipid metabolites from bisphenol S-induced nephrotoxicity. *Anal. Chem.* **90**(5), 3196–3204. <https://doi.org/10.1021/acs.analchem.7b04540> (2018).
45. Zhang, R., Liu, R. & Zong, W. Bisphenol, W. Interacts with catalase and induces oxidative stress in mouse liver and renal cells. *J. Agric. Food Chem.* **64**(34), 6630–6640. <https://doi.org/10.1021/acs.jafc.6b02656> (2016).
46. Peretz, J. et al. Bisphenol A and reproductive health: update of experimental and human evidence, 2007–2013. *Environ. Health Perspect.* **122**(8), 775–786. <https://doi.org/10.1289/ehp.1307728> (2014). Epub 2014 Jun 4.
47. Kobroob, A., Peerapanyasut, W., Chattipakorn, N. & Wongmekiat, O. Damaging effects of bisphenol A on the kidney and the protection by melatonin: Emerging evidences from in vivo and in vitro studies. *Oxid Med Cell Longev* **2018**, 3082438. <https://doi.org/10.1155/2018/3082438> (2018).
48. Jacobson, M. H. et al. Serially assessed bisphenol A and phthalate exposure and association with kidney function in children with chronic kidney disease in the US and Canada: A longitudinal cohort study. *PLoS Med.* **17**(10), e1003384. <https://doi.org/10.1371/journal.pmed.1003384> (2020).
49. Li, G. et al. Long-term exposure to ambient PM2.5 and increased risk of CKD prevalence in China. *J. Am. Soc. Nephrol.* **32**(2), 448–458. <https://doi.org/10.1681/ASN.2020040517> (2021).
50. Wu, C. T., Wang, C. C., Huang, L. C., Liu, S. H. & Chiang, C. K. Plasticizer Di-(2-Ethylhexyl)Phthalate induces Epithelial-to-Mesenchymal transition and renal fibrosis in vitro and in vivo. *Toxicol. Sci.* **164**(1), 363–374. <https://doi.org/10.1093/toxsci/kfy094> (2018).
51. Shihab, F. S. Do we have a pill for renal fibrosis? *Clin. J. Am. Soc. Nephrol.* **2**(5), 876–878. <https://doi.org/10.2215/CJN.02660707> (2007).

52. Efstratiadis, G., Divani, M. & Katsioulis, E. Vergoulas. Renal fibrosis. *Hippokratia* **13**(4), 224–229 (2009).
53. Whiteman, E. L., Liu, C. J., Fearon, E. R. & Margolis, B. The transcription factor snail represses Crumbs3 expression and disrupts apico-basal polarity complexes. *Oncogene* **27**(27), 3875–3879. <https://doi.org/10.1038/ncr.2008.9> (2008).
54. Chen, A. et al. E-cadherin loss alters cytoskeletal organization and adhesion in non-malignant breast cells but is insufficient to induce an epithelial-mesenchymal transition. *BMC Cancer*. **14**, 552. <https://doi.org/10.1186/1471-2407-14-552> (2014).
55. Bauer, H., Zweimüller-Mayer, J., Steinbacher, P., Lametschwandner, A. & Bauer, H. C. The dual role of zonula occludens (ZO) proteins. *J. Biomed. Biotechnol.* **2010**, 402593. <https://doi.org/10.1155/2010/402593> (2010).
56. Matter, K. & Balda, M. S. Epithelial tight junctions, gene expression and nucleo-junctional interplay. *J. Cell Sci.* **120**(Pt 9), 1505–1511. <https://doi.org/10.1242/jcs.005975> (2007).
57. Mendez, M. G., Kojima, S. & Goldman, R. D. Vimentin induces changes in cell shape, motility, and adhesion during the epithelial to mesenchymal transition. *FASEB J.* **24**(6), 1838–1851. <https://doi.org/10.1096/fj.09-151639> (2010).
58. Lee, J. M., Dedhar, S., Kalluri, R. & Thompson, E. W. The epithelial-mesenchymal transition: New insights in signaling, development, and disease. *J. Cell. Biol.* **172**(7), 973–981. <https://doi.org/10.1083/jcb.200601018> (2006).
59. Loh, C. Y. et al. E-Cadherin and N-Cadherin switch in Epithelial-to-Mesenchymal transition: Signaling, therapeutic Implications, and challenges. *Cells* **8**(10), 1118. <https://doi.org/10.3390/cells8101118> (2019).
60. Wen, Q. & Janmey, P. A. Polymer physics of the cytoskeleton. *Curr. Opin. Solid State Mater. Sci.* **15**(5), 177–182. <https://doi.org/10.1016/j.cossms.2011.05.002> (2011).
61. Shankar, J., Messenberg, A., Chan, J., Underhill, T. M., Foster, L. J. & Nabi, I. R. Pseudopodial actin dynamics control epithelial-mesenchymal transition in metastatic cancer cells. *Cancer Res.* **70**(9), 3780–3790. <https://doi.org/10.1158/0008-5472.CAN-09-4439> (2010).
62. Yilmaz, M. & Christofori, G. EMT, the cytoskeleton, and cancer cell invasion. *Cancer Metastasis Rev.* **28**(1–2), 15–33. <https://doi.org/10.1007/s10555-008-9169-0> (2009).
63. Roll-Mecak, A. T. Tubulin code in microtubule dynamics and information encoding. *Dev. Cell.* **54**(1), 7–20. <https://doi.org/10.1016/j.devcel.2020.06.008> (2020).
64. Janke, C. & Magiera, M. M. The tubulin code and its role in controlling microtubule properties and functions. *Nat. Rev. Mol. Cell. Biol.* **21**(6), 307–326. <https://doi.org/10.1038/s41580-020-0214-3> (2020).
65. Wei, Y. et al. Polystyrene microplastics disrupt the blood-testis barrier integrity through ROS-Mediated imbalance of mTORC1 and mTORC2. *Environ. Pollut.* **289**, 117904. <https://doi.org/10.1016/j.envpol.2021.117904> (2021).
66. Zhang, H. et al. Bisphenol S promotes clear cell renal cell carcinoma progression by modulating the WNT5A-dependent EMT pathway. *Toxicology* **514**, 154117. <https://doi.org/10.1016/j.tox.2025.154117> (2025). Epub 2025 Mar 12.
67. Yang, H. et al. Transplantation of Wnt5a-modified bone marrow mesenchymal stem cells promotes recovery after spinal cord injury via the PI3K/AKT pathway. *Mol. Neurobiol.* **61**(12), 10830–10844. <https://doi.org/10.1007/s12035-024-04248-8> (2024). Epub 2024 May 25.
68. Xue, M. et al. Attenuates renal tubular Epithelial-mesenchymal transition via the MiR-188-5p-mediated PI3K/AKT pathway in diabetic kidney disease. *Int. J. Biol. Sci.* **14**(11), 1545–1557. <https://doi.org/10.7150/ijbs.24032> (2018).
69. Shin, J. H. et al. Nrf2-heme oxygenase-1 attenuates high-glucose-induced epithelial-to-mesenchymal transition of renal tubule cells by inhibiting ROS-mediated PI3K/Akt/GSK-3β signaling. *J. Diabetes Res.* **2019**, 2510105. <https://doi.org/10.1155/2019/2510105> (2019).
70. Xu, Z. et al. METTL14-regulated PI3K/Akt signaling pathway via PTEN affects HDAC5-mediated epithelial-mesenchymal transition of renal tubular cells in diabetic kidney disease. *Cell. Death Dis.* **12**(1), 32. <https://doi.org/10.1038/s41419-020-03312-0> (2021).
71. Shimobayashi, M. & Hall, M. N. Making new contacts: The mTOR network in metabolism and signalling crosstalk. *Nat. Rev. Mol. Cell. Biol.* **15**(3), 155–162. <https://doi.org/10.1038/nrm3757> (2014).
72. Lu et al. Quercetin inhibits the mTORC1/p70S6K signaling-mediated renal tubular epithelial-mesenchymal transition and renal fibrosis in diabetic nephropathy. *Pharmacol. Res.* **99**, 237–247. <https://doi.org/10.1016/j.phrs.2015.06.006> (2015).
73. Hou, L. et al. B1 induces nephrotoxicity via autophagy mediated by mTORC1 instead of mTORC2 in human renal tubule epithelial cells. *Food Chem. Toxicol.* **149**, 112037. <https://doi.org/10.1016/j.fct.2021.112037> (2021).
74. Li, J. et al. Rictor/mTORC2 signaling mediates TGFβ1-induced fibroblast activation and kidney fibrosis. *Kidney Int.* **88**(3), 515–527. <https://doi.org/10.1038/ki.2015.119> (2015).
75. Li, J. et al. Rictor/mTORC2 protects against cisplatin-induced tubular cell death and acute kidney injury. *Kidney Int.* **86**(1), 86–102. <https://doi.org/10.1038/ki.2013.559> (2014).
76. Gao, Q. et al. mTORC2 regulates hierarchical micro/nano topography-induced osteogenic differentiation via promoting cell adhesion and cytoskeletal polymerization. *J. Cell. Mol. Med.* **25**(14), 6695–6708. <https://doi.org/10.1111/jcmm.16672> (2021).
77. Sarbassov, D. D. et al. Rictor, a novel binding partner of mTOR, defines a rapamycin-insensitive and raptor-independent pathway that regulates the cytoskeleton. *Curr. Biol.* **14**(14), 1296–1302. <https://doi.org/10.1016/j.cub.2004.06.054> (2004).
78. Jeong, Y. J., Hwang, S. K., Magae, J. & Chang, Y. C. Ascofuranone suppresses invasion and F-actin cytoskeleton organization in cancer cells by inhibiting the mTOR complex 1 signaling pathway. *Cell. Oncol. (Dordr.)* **43**(5), 793–805. <https://doi.org/10.1007/s13402-020-00520-w> (2020).

## Acknowledgements

Not applicable.

## Author contributions

Zhaoxia Zhang: Conceptualization, visualization, writing—original draft. Liming Jin: Investigation, data curation, visualization, software. Tao Mi: Data curation, visualization, software. Jinkui Wang: Methodology, software. Zhaoying Wang: Methodology, visualization. Chunlian Ren: Investigation, data curation. Xin Wu: Methodology, validation. Jiayan Liu: Investigation, validation. Peng Guo: Writing—editing. Li wang and Dawei He: Conceptualization, funding acquisition, project administration.

## Funding

This study was supported by grants from Chongqing Talent Program “lump sum project” (cstc2021ycjh-bg-zxm0253) and Chongqing Science and Health Joint Project (2023GDRC009).

## Declarations

## Ethics approval and consent to participate

All experimental procedures involving animals were performed in accordance with the Basel Declaration

and were approved by the Ethics Committee. All experimental animal procedures used in the study were approved by the Ethics Committee of the Children's Hospital of Chongqing Medical University (IACUC Issue NO: CHCMU-IACUC20220323004). All procedures were conducted in full compliance with the ARRIVE guidelines. All methods were carried out in accordance with relevant guidelines and regulations.

### Competing interests

The authors declare no competing interests.

### Additional information

**Supplementary Information** The online version contains supplementary material available at <https://doi.org/10.1038/s41598-025-30100-7>.

**Correspondence** and requests for materials should be addressed to L.W. or D.H.

**Reprints and permissions information** is available at [www.nature.com/reprints](http://www.nature.com/reprints).

**Publisher's note** Springer Nature remains neutral with regard to jurisdictional claims in published maps and institutional affiliations.

**Open Access** This article is licensed under a Creative Commons Attribution-NonCommercial-NoDerivatives 4.0 International License, which permits any non-commercial use, sharing, distribution and reproduction in any medium or format, as long as you give appropriate credit to the original author(s) and the source, provide a link to the Creative Commons licence, and indicate if you modified the licensed material. You do not have permission under this licence to share adapted material derived from this article or parts of it. The images or other third party material in this article are included in the article's Creative Commons licence, unless indicated otherwise in a credit line to the material. If material is not included in the article's Creative Commons licence and your intended use is not permitted by statutory regulation or exceeds the permitted use, you will need to obtain permission directly from the copyright holder. To view a copy of this licence, visit <http://creativecommons.org/licenses/by-nc-nd/4.0/>.

© The Author(s) 2025